Contrib Mineral Petrol (1999) 137: 232–245 

**Marthinus Cloete · Rodger J. Hart · Herbert K. Schmid**
**Martyn Drury · Chris M. Demanet · K. Vijaya Sankar**

# Characterization of magnetite particles in shocked quartz by means of electron- and magnetic force microscopy: Vredefort, South Africa

Received: 16 November 1998 / Accepted: 17 May 1999

**Abstract** Submicroscopic opaque particles from highly shocked granite-gneisses close to the core of the Vredefort impact structure have been investigated by means of micro-analytical techniques with high spatial resolution such as electron diffraction, orientation contrast imagery and magnetic force microscopy. The opaque particles have been identified as nano- to micro-sized magnetite that occur in several distinct modes. In one sample magnetite occurs along relict planar deformation features (PDFs) in quartz, generally accepted as typical shock lamellae. The magnetite particles along shock lamellae in quartz grains virtually all show uniform crystallographic orientations. In most instances, the groups of magnetite within different quartz grains are systematically misorientated such that they share a subparallel ⟨101⟩ direction. The magnetite groups of all measured quartz grains thus appear to have a crystallographic preferred orientation in space. In a second sample, orientations of magnetite particles have been measured in microfractures (non-diagnostic of shock) of quartz, albite and in the alteration halos, (e.g. biotite grains breaking down to chlorite). The crystallographic orientations of magnetite particles are diverse, with only a minor portion having a preferred orientation. Scanning electron microscopy shows that magnetite along the relict PDFs is invariably associated with other microcrystalline phases such as quartz, K-feldspar and biotite. Petrographic observations suggest that these microcrystalline phases crystallized from locally formed micro-melts that intruded zones of weakness such as microfractures and PDFs shortly after the shock event. The extremely narrow widths of the PDFs suggest that heat may have dissipated rapidly resulting in melts crystallizing relatively close to where they were generated. Magnetic force microscopy confirms the presence of magnetic particles along PDFs. The smallest particles, $<5$ μm with high aspect ratios 15:1 usually exhibit intense, uniform magnetic signals characteristic of single-domain magnetite. Consistent offsets between attractive and repulsive magnetic signals of individual single-domain particles suggest consistent directions of magnetization for a large proportion of particles.

M. Cloete · R.J. Hart
Council for Geoscience,
Private Bag X112, Pretoria, RSA

R.J. Hart
Schonland Research Centre, Wits University,
P.O. Box 3, Johannesburg 2050

H.K. Schmid[1]
Division of Materials Science and Technology, CSIR,
P.O. Box 395, Pretoria 0001

M. Drury
Department of Geology, Faculty of Earth Sciences,
Utrecht University, P.O. Box 80.021,
3508TA Utrecht, Netherlands

C.M. Demanet · K. Vijaya Sankar
Department of Physics, University of Transkei,
Private Bag X1, Umtata 5100, South Africa

*Present address*:
[1] Institut für Neue Materialien,
Im Stadtwald 43, D-66123 Saarbrücken, Germany

Editorial responsibility: T.L. Grove

## Introduction

The origin of the Vredefort structure in South Africa, whether by asteroid impact, internal gas explosion or tectonic processes, is controversial (Nicolaysen and Reimold 1990). The morphology of the structure (Fig. 1) resembles that expected of deep central zone of a large complex crater (current estimates suggest an original diameter of ~300 km, Therriault et al. 1993). The margin of the remnant structure consists of a semicircular series of ridges of Precambrian strata, surrounding a central flat area consisting mainly of Archean granitic basement. The occurrence of shatter cones (Albat 1988; Hargraves 1961), planar deformation defects (Grieve et al. 1990; Leroux et al. 1994) and high-pressure quartz polymorphs, e.g., coesite and stishovite (Martini 1991), are interpreted as evidence of dynamic rock deformation caused by an impact event at Vredefort.

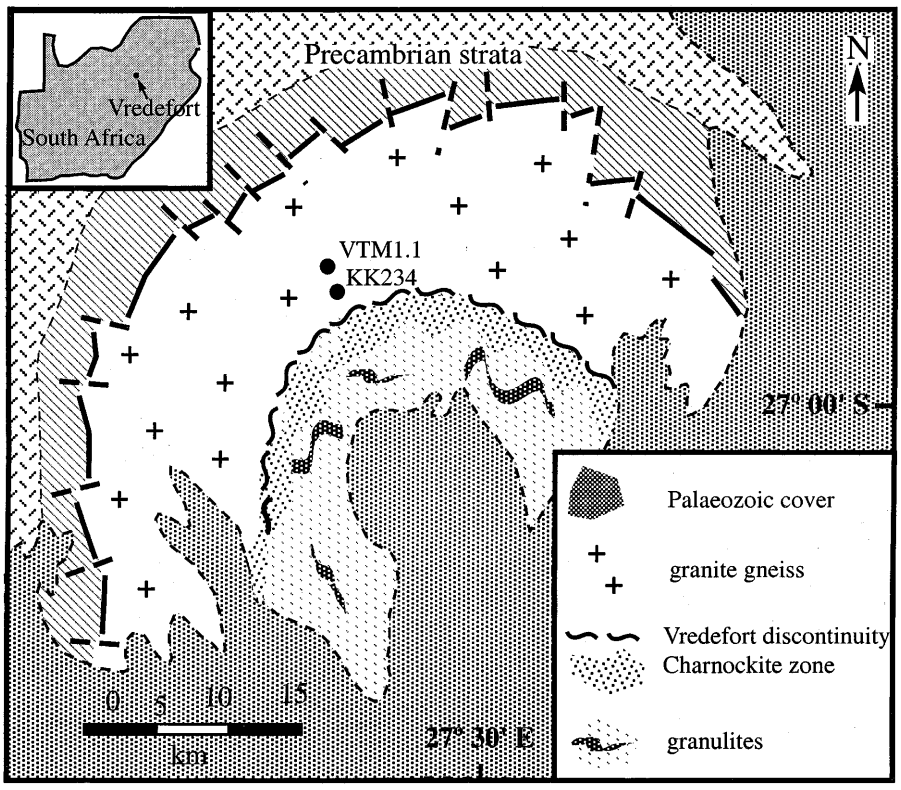


**Fig. 1** Simplified geological map of Vredefort structure showing sample localities (after Hart et al. 1990)

Much of the controversy regarding the origin of the Vredefort structure has centred around the nature and distribution of the deformation phenomena related to the dynamic metamorphism, and in particular planar deformation features (PDFs) and fractures in quartz that mainly occur in the central granitic basement. This controversy is discussed in detail by Carter et al. (1990), Grieve et al. (1990), Reimold (1990) and Leroux et al. (1994). The authors cited conclude that Vredefort PDFs are anomalous compared to those at other known impact structures, with respect to their relative distribution, preservation and orientations. Variations in the recorded shock pressures, calculated on the basis of the distribution of planar features, are shown not to regularly decrease outwards as observed at other impact structures. Also, some of the most frequently observed PDF-orientations for all impact sites, in decreasing order of abundance, are $[10\bar{1}3]$, $[10\bar{1}2]$, $[10\bar{1}1]$ and [0001] (from a total of fifteen, listed by Grieve et al., 1996). At Vredefort, 90% of all PDFs studied exhibit basal orientations, which are mechanical twins of the Brazil type. At Vredefort, the $(10\bar{1}3)$ and $(10\bar{1}2)$ orientations have also been observed (Fricke et al. 1990; Grieve et al 1990) but are considered to be relatively rare. As a consequence, many workers have concluded that the somewhat anomalous evidence of the PDFs is still consistent with the Vredefort structure being an eroded remnant of a large complex impact structure (Grieve et al. 1990; Leroux et al. 1994).

Many of the PDFs at Vredefort differ from those in other large impact structures, in that they have been recrystallized, and are also occasionally decorated along their length by submicroscopic opaque dust (Hart et al. 1991; Grieve et al. 1990). Since much of the recrystallized rocks and the opaque phases in these rocks occur as a fine-grained microscopic material, positive identification of these particles could not be achieved in normal petrographic examinations, because the mean particle size ($<1$ μm) is below the resolution limit of routine instruments.

In this study, we provide a detailed observation of the microstructure, crystallography and composition of mineral phases along the PDFs in quartz by means of transmission electron microscopy/scanning transmission electron microscope (TEM/STEM) techniques. To overcome the logistical problem inherent in using TEM/STEM to record information over larger areas ($>3$ mm), continuous measurements were made with a scanning electron microscope (SEM using electron backscatter diffraction and orientation contrast imaging of forescatter electrons (Prior et al. 1996). Finally, the technique of magnetic force microscopy (MFM) was used to confirm qualitative data on the shape, size and magnetic properties of the multi- and single-domain magnetite particles.

## Sample locality and analytical details

Two samples (KK 234 and VTM1.1) of granite-gneiss (see Fig. 1. for locality) were collected from the basement core of the Vredefort structure for studies by TEM/SEM. Both samples are collected in a

region characterized by rocks with an unusually high remnant magnetism and a high frequency of planar deformation features in quartz (Hart et al. 1991, 1995). Preliminary petrographic study, however, showed the two samples to be distinctly different. KK234 contains quartz grains with *bona fide* PDF, which locally bear opaque oxides (Fig. 2); whereas, VTM1.1 exhibits only microfractures (non-diagnostic of shock) and has silicate phases with minor opaque dusts.

### Transmission electron microscopy

Electron transparent thin foils for TEM investigations of sample KK234 were prepared using standard preparation methods for ceramic materials. Sample areas of interest, containing opaque inclusions in quartz grains, were selected by drilling discs 3 mm in diameter from ~100 μm thick doubly polished petrographic wafers using an ultrasonic core drill. The specimens were further thinned by mechanical dimple grinding/polishing followed by Ar ion-beam etching (5–12 kV Ar, 12°) till perforation. The thinning process resulted in exposing numerous nano-sized magnetite particles situated in two differently oriented quartz grains, as well as in a pocket of amorphous silica suitable for investigations in a 120 kV Philips EM 420 analytical TEM/STEM equipped with EDS and EELS attachments for microchemical analysis with high spatial resolution (~10 nm). The crystallography of large features (>1 μm) could be analysed by conventional selected area electron diffraction (SAD); whereas, submicron sized particles were analysed by micro-diffraction techniques (μD mode in STEM and μD in TEM respectively). The structure of quartz was used as internal standard for calibration (a = 0.49133 nm, c = 0.54053 nm; PDF # 33–1161 (JCPDS, ASTM 1994).

### Scanning electron microscopy

Most of the work was done on a Philips XL30 FEG SEM. The orientation contrast images were taken with a normal backscatter detector but in the forward scattering position, with the specimen tilted to 70 degrees (Prior et al. 1996). Specimen preparation involved polishing to microprobe grade, and then with colloidal silica (Syton) on a hard foam polishing wheel (Malvern instruments Multipol 2).

The operating conditions were 15–20 kV using spot size 4–5, which corresponds to probe currents of about 0.5 nA. A working distance of 15 mm was used and all specimens were uncoated. The orientation measurements were done by indexing electron backscattered patterns (Prior et al. 1996), using the channel + software from *hkl* technology in Denmark.

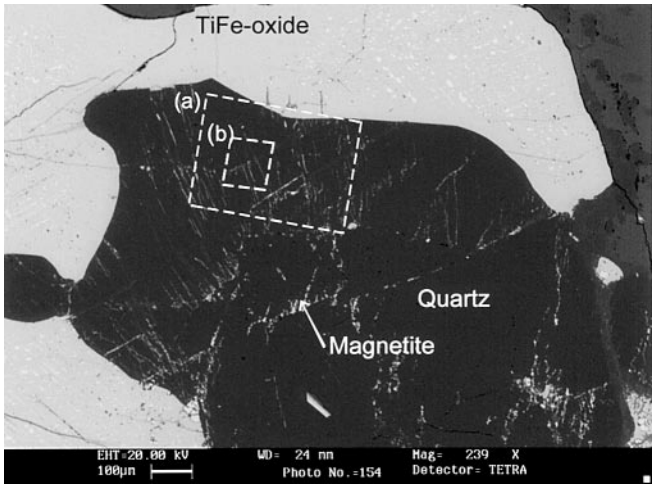


**Fig. 2** Backscatter image showing a typical example of quartz containing sub-parallel sets of lamellae- and microfracture magnetite. The insert boxes *a* and *b* show the position of Figs. 14 and 18, i.e., main areas of interest discussed in the text. Width of field of view = 1.5 mm

### Magnetic force microscopy

Micron-sized grains of magnetite in sample KK234 have been analysed by means of MFM. An approximately 80-μm thick wafer of rock was prepared as a thin section, using standard petrographic techniques, and polished with diamond suspension to obtain a smooth surface.

MFM stems from atomic force microscope (AFM, Martin and Wickramasinghe 1987; Grutter et al. 1992; Grütter and Allenspach 1994; Pokhil and Moskowitz 1997) and utilizes a sharp magnetic tip attached to a flexible cantilever. The tip is placed close to the sample surface (10–100 nm) and interacts with the magnetic stray field emanating from the sample. The image is generated by scanning the tip laterally in relation to the sample and measuring the magnetic force or force gradient, as a function of position.

An Autoprobe CP from Park Scientific Instruments equipped with a piezo-scanner of maximum lateral scan size of 100 μm was used. All images were acquired in air at ambient conditions. The images were acquired using a magnetised Co coated Si tip, with a length of about 3 mm. Magnetization was achieved by placing the tip in the field of a magnet in a direction parallel to the field lines, such that the tip has a polarization normal to the scanned sample surface. Topographic (or AFM) and magnetic force images were acquired simultaneously, thus, ensuring perfect registration of features by recording the a.c. and d.c. signals. The images were acquired at slow scan rates of 0.5 or 0.2 Hz and at a resolution of 256 pixel per line.

The magnetic force images are coded in grey scale (and colour) with dark regions (blue and purple) reflecting an attractive force, where the cantilever is pulled towards the sample. Lighter regions (yellow and orange) reflect a repulsive force, where the cantilever is deflected away from the surface as a result of the magnetic interaction between the tip and magnetic regions in the sample. The tip to surface distance was typically between 10 and 40 nm. The topographic and magnetic images at large scan size (>50 μm) were flattened, using a second-order polynomial in the X and Y directions to compensate for the bowing of the piezo tube. A 0th order fit was performed on magnetic force images of scan size larger than 50 mm, to match the average grey scale of each line in the image. In some cases, a ripple structure in the magnetic force images, appearing as a distinct frequency on a Fast Fourier Transformed representation, was also filtered out.

## TEM/STEM results

### Microstructure/microchemistry

A perforated specimen of sample KK234 was analysed in detail by TEM/STEM techniques (Fig. 3a). The sizes of the magnetite grains projecting from the edge of the perforated thin foil vary from 2–5 μm. STEM X-ray mapping (Fig. 3) shows the distribution of Fe, Ti and Ca cations. The extent of the magnetite grains is clearly outlined by the Fe distribution in the X-ray map. Some inclusions showed high concentrations of Ti, Ca and Si (titanite); whereas, the concentration of Fe in these particles was rather low (<1.5 at.%). Quantitative EDS spot analyses of individual magnetite grains indicated an atomic concentration for Fe > 98% with traces of Ti between 0.7 and 1.5 at.%.

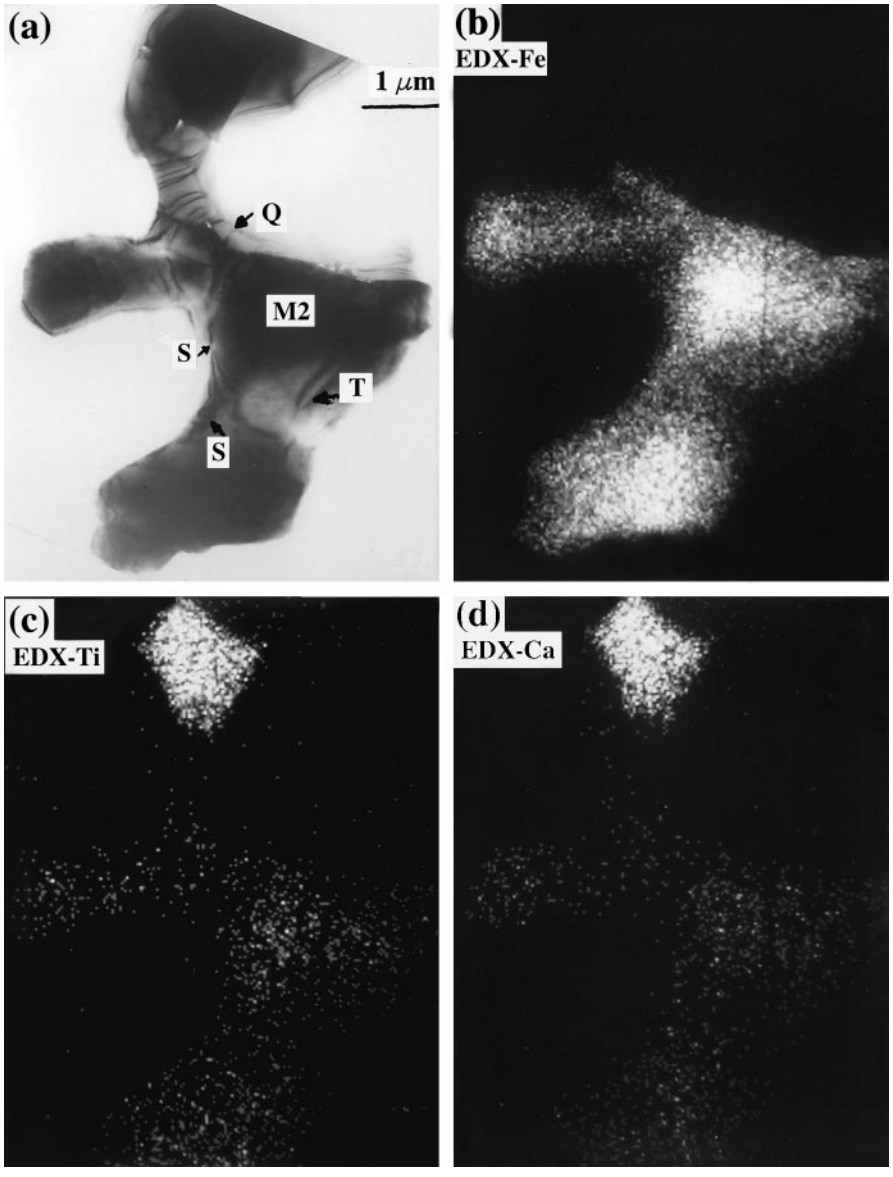


**Fig. 3 a** A typical magnetite grain (*M2*) protruding over the edge of a quartz grain (*Q*); magnetite grain shows twin (*T*) and sub-grain (*S*) boundaries (TEM-Bright Field image). **b–d** Element mapping in STEM showing Fe, Ti and Ca distribution in magnetite grains (*M*) and titanate grains

Images at higher magnification revealed the existence of submicron particles dispersed in quartz grains in the vicinity of larger magnetite grains (Fig. 4). These inclusions vary in size from ~10–100 nm in diameter for the equiaxed particles. Some particles appear elongated with aspect ratio up to 5:1. In tilting experiments, the particles give rise to strong diffraction contrasts under certain specimen orientations with respect to the incident electron beam, revealing their crystalline nature. The size of the small magnetite particles is near the practical resolution limit for X-ray mapping in the STEM system used (256 × 200 pixel frame; pixel size 20 × 20 nm; acquisition time 150 ms/pixel); thus, particles with diameters <50 nm are recognized with some difficulty in Fe maps (Fig. 5). The large magnetite grains numbered (1) and (3) in the STEM images are clearly separated by an intergranular film approximately 0.05 μm thick (Fig. 6). Although the bulk of both the quartz grains and the opaque inclusions are crystalline, small patches of silica and iron oxide in an amorphous or paracrystalline state have been observed in interface regions between large magnetite grains and host quartz (Figs. 4 and 6). The paracrystalline material (P) shows a lamellar structure.

## Crystallography

The crystal structure of a large number of magnetite grains from sample KK234 have been investigated by electron diffraction techniques for phase identification, as well as to establish their crystallographic orientations in relation to their quartz hosts. Using quartz as internal standard for calibrating the camera constant, both large opaque grains and nm-sized inclusions could be unambiguously identified as magnetite (a = 0.8396 nm, PDF # 19–629 (JCPDS, ASTM 1994), though the ob-

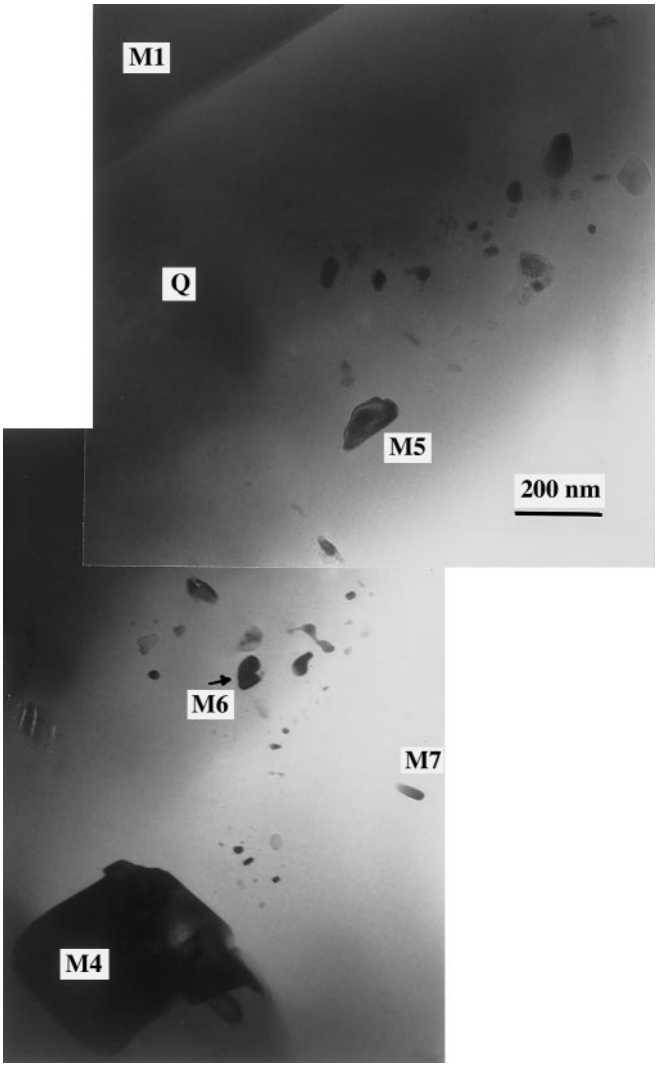


**Fig. 4** TEM-Bright Field image showing *M* in *Q*; Magnetite particle M7 is in amorphous silica

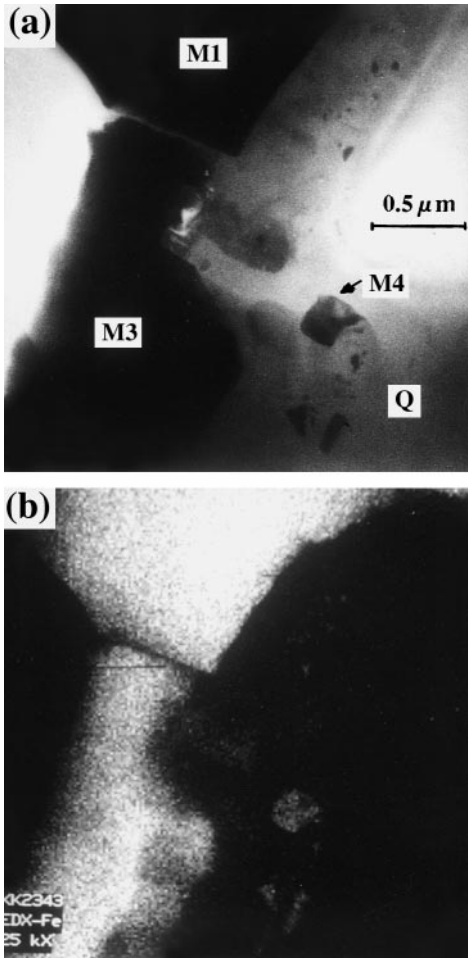


**Fig. 5a, b** STEM images of *M* in *Q*; **a** bright-field image, **b** Fe-K signal showing distribution of Fe in magnetite

servation of additional reflections [001], [002], [110], [102], [112] (Fig. 7a), unacceptable in an fcc structure by the selection rules for a system with space group Fd3 m, (#227, Int. Tables for X-ray Cryst. 1965), initially caused some confusion. However, some of the larger magnetite grains showed twinning, identified in [110] zone-axis SAD patterns as $(\bar{1}11)$ twins (twin plane parallel to electron beam; $[\bar{1}11]$ twin axis (Fig. 8b, c). Occasionally, individual unrelated magnetite grains situated in the host quartz at some distance from each other have been observed in exact twin orientation relationship, i.e. the orientation of one particle, with respect to the other, is inverted by a 180° rotation about a common $\langle 111 \rangle$ axis, as indicated (Fig. 7b, c). High resolution imaging confirmed that none of these twin-related magnetite particles contained any twin boundary.

All the magnetite inclusions analysed in quartz are oriented with [110] of magnetite parallel to $[\bar{1}100]$ of quartz. Two different orientation relationships (orientations I and II), respectively have been observed. The majority of magnetite inclusions were observed in orientations characterized by:

$$\begin{aligned} &[\bar{3}\bar{3}2] \,||\, [0001] \\ \text{and} \quad &(\bar{1}10) \,||\, (\bar{1}100) \\ &(113) \,||\, (11\bar{2}0), \end{aligned}$$

as indicated in the stereographic projection (Fig. 8a). The corresponding diffraction patterns are shown (Fig. 8b, c). It was noted that large particles showed a slight deviation (average deviation angle ~3°) from an exact orientation (I), as indicated in the schematic diagram (Fig. 8d). Twin variants of magnetite (i.e. rotated 180° about $[\bar{1}11]$) were observed in exact orientation (II) characterized by:

$$\begin{aligned} &[111] \,||\, [\bar{1}\bar{1}20] \\ \text{and} \quad &(01\bar{1}) \,||\, (\bar{1}100) \\ &(2\bar{1}\bar{1}) \,||\, (0001), \end{aligned}$$

as indicated in Fig. 9. In this orientation relationship, two sets of [110], $[1\bar{1}02]$ and $[1\bar{1}3]$, $[1\bar{2}10]$ planes deviate from parallelism by angles 2.4° and 0.5°, respectively.

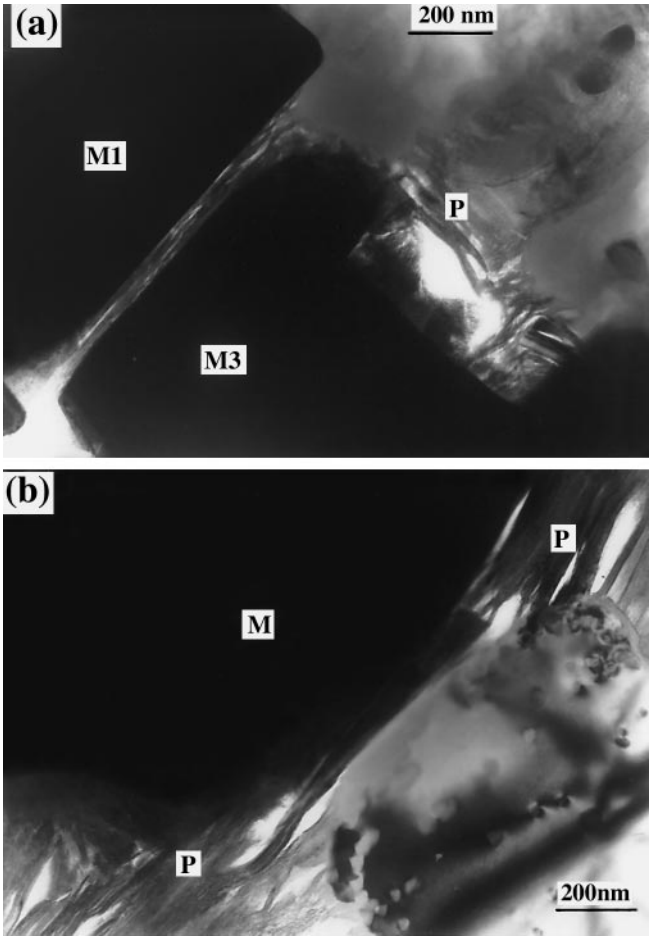


**Fig. 6a, b** TEM-Bright Field images showing amorphous and paracrystalline material (*P*) in interface regions between large *M* and quartz; paracrystalline silica (**a**), and paracrystalline iron oxide (**b**) both show lamellae structure

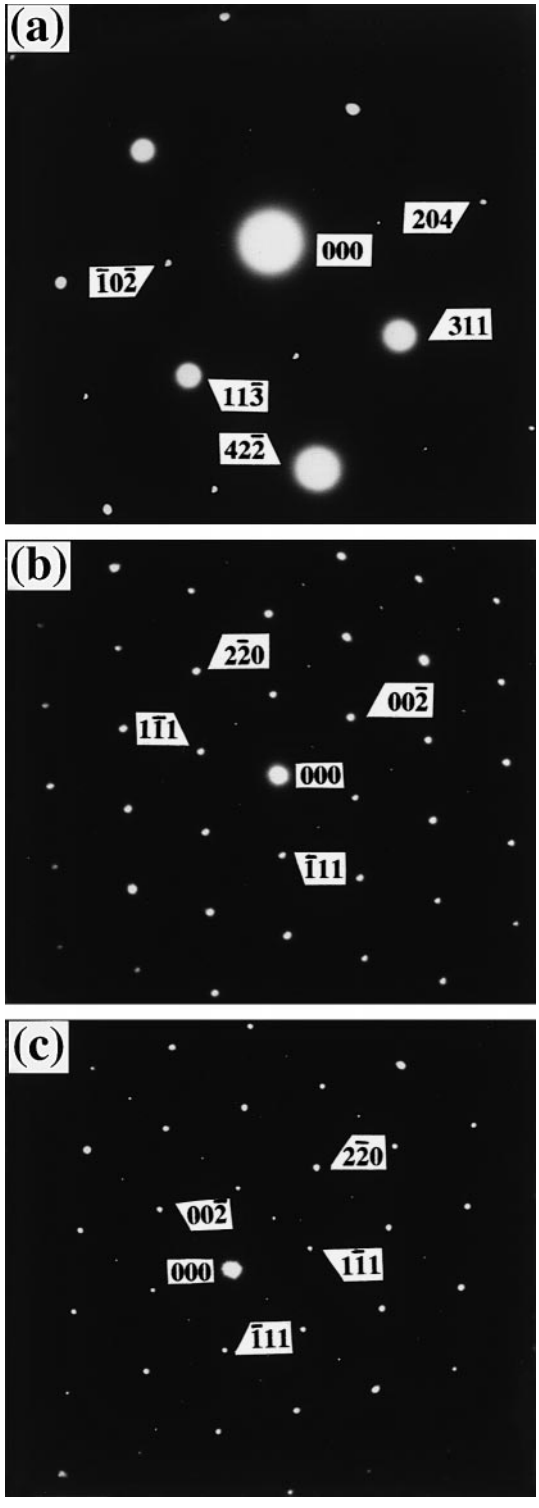


**Fig. 7a–c** Electron diffraction patterns of magnetite show forbidden reflections; **a** zone axis ZA = [51]; **b** ZA = [0]; **c** ZA = [110] twin orientation (*T*)

By recording the tilt angles on the goniometer stage for crystal orientations, it was noted that regardless of the relative orientation of the quartz grains all magnetite grains were approximately in the same orientation in sample KK234. The goniometer tilt angles measured relative to the orientation of the [0001] zone-axis of the largest quartz grain are indicated schematically in Fig. 10 for the $[1\bar{1}0]$ zone-axis of selected magnetite particles, 1 to 5 (orientation I), as well as twin orientation T (orientation II). A majority of magnetite grains were found in orientations clustering around the orientation of particle #5. Greater deviations from this orientation up to 5°, were observed for some large magnetite grains (e.g., grain #2) and twin variants in orientation II.

After further ion milling of the sample, in order to obtain electron transparent thin areas in a large number of differently orientated quartz grains, five more iron oxide particles were analysed. Four particles have been positively identified as magnetite; whereas, one particle appeared to be maghemite (PDF 39–1346). Again, [110] of magnetite was oriented approximately parallel to [1100] of the host quartz. There is no special crystallographic orientation relationship between magnetite and host lattice in this quartz. One of the magnetite particles also showed an exact twin orientation relationship, with respect to the others. Whether the orientations of these particles are the same as the orientations of the particles

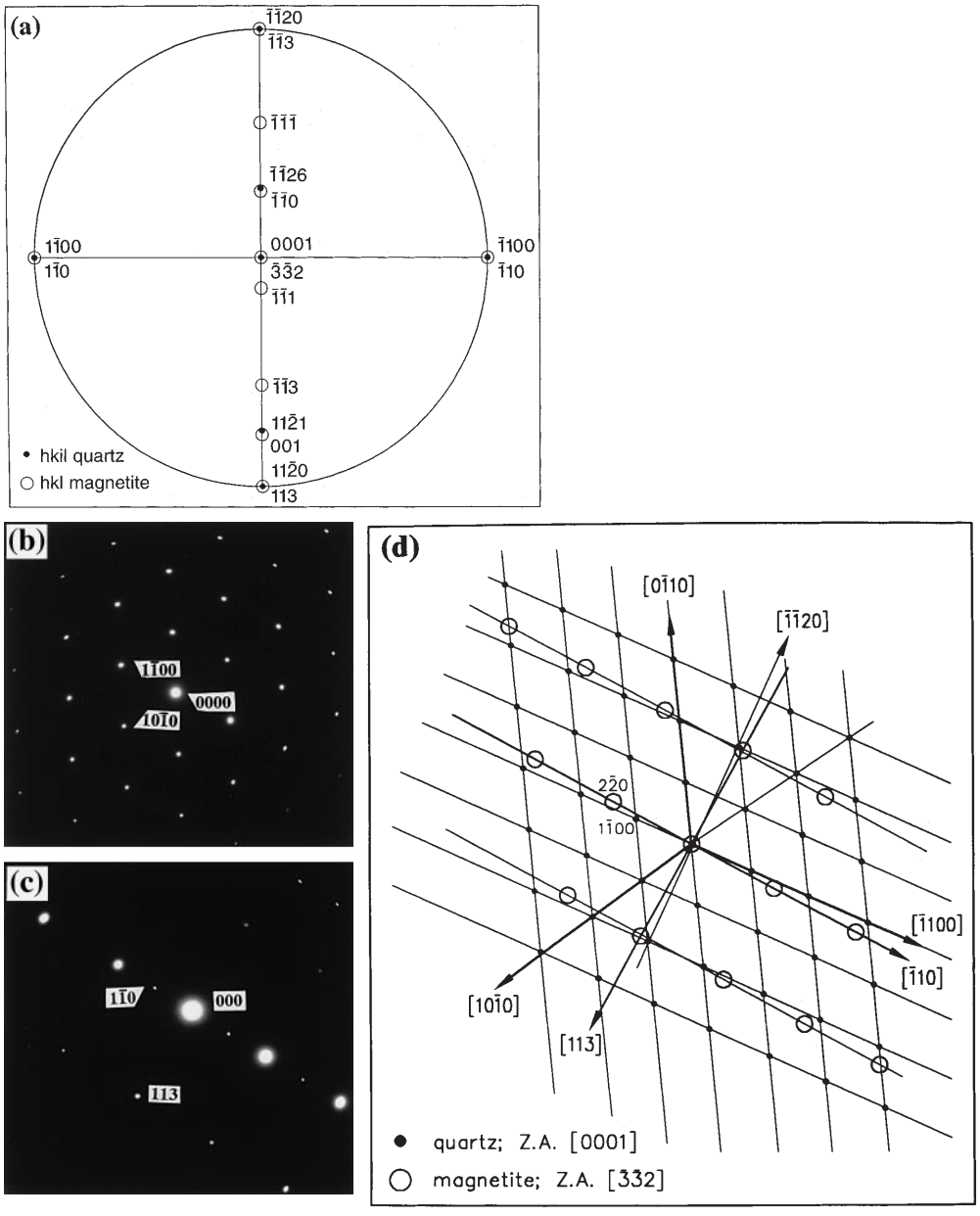


**Fig. 8** **a** Stereographic projection representing orientation relationship I between quartz and magnetite inclusions; **b** electron diffraction pattern of quartz, ZA [0001]; **c** electron diffraction pattern of magnetite, ZA = [2]; **d** schematic diagram of reciprocal lattice coincidences

analysed prior to the re-milling of the sample (i.e., whether all magnetite particles adopt a uniform orientation irrespective of orientation of their quartz hosts) could not be unambiguously established.

## SEM results

Sample KK234

The magnetite particles investigated by SEM occur along linear arrays presumed to be PDFs. Although the quartz around the magnetite particles is invariably recrystallized (Figs. 11 and 12), such that the original lamellae are no longer recognizable, the planes along which the magnetite particles are occur, viz: (0001), $(10\bar{1}3)$ and $(10\bar{1}2)$, are identical to those of the *bona fide* PDFs in quartz (e.g., Grieve et al. 1990). The magnetite particles range from equant to elongate, i.e., have aspect ratios between approximately 1 and 15 with maximum width generally $< 1$ μm and length 0.5–8 μm.

Electron diffraction measurements show the magnetite particles in any quartz grain to have identical orientations. The [100] and [101] poles of magnetite particles from three quartz grains; A (10 particles), B (4 particles) and C (1 particle) were found to be uniform with respect to their hosts, but have high angles of variance between one quartz grain and another (Fig 13a, b). The misorientations between A and B = 50.2°, and between A and C = 56.6° whereas between B and C = 49.1°. Despite the high degree of misorientations between the groups of magnetite particles, they appear

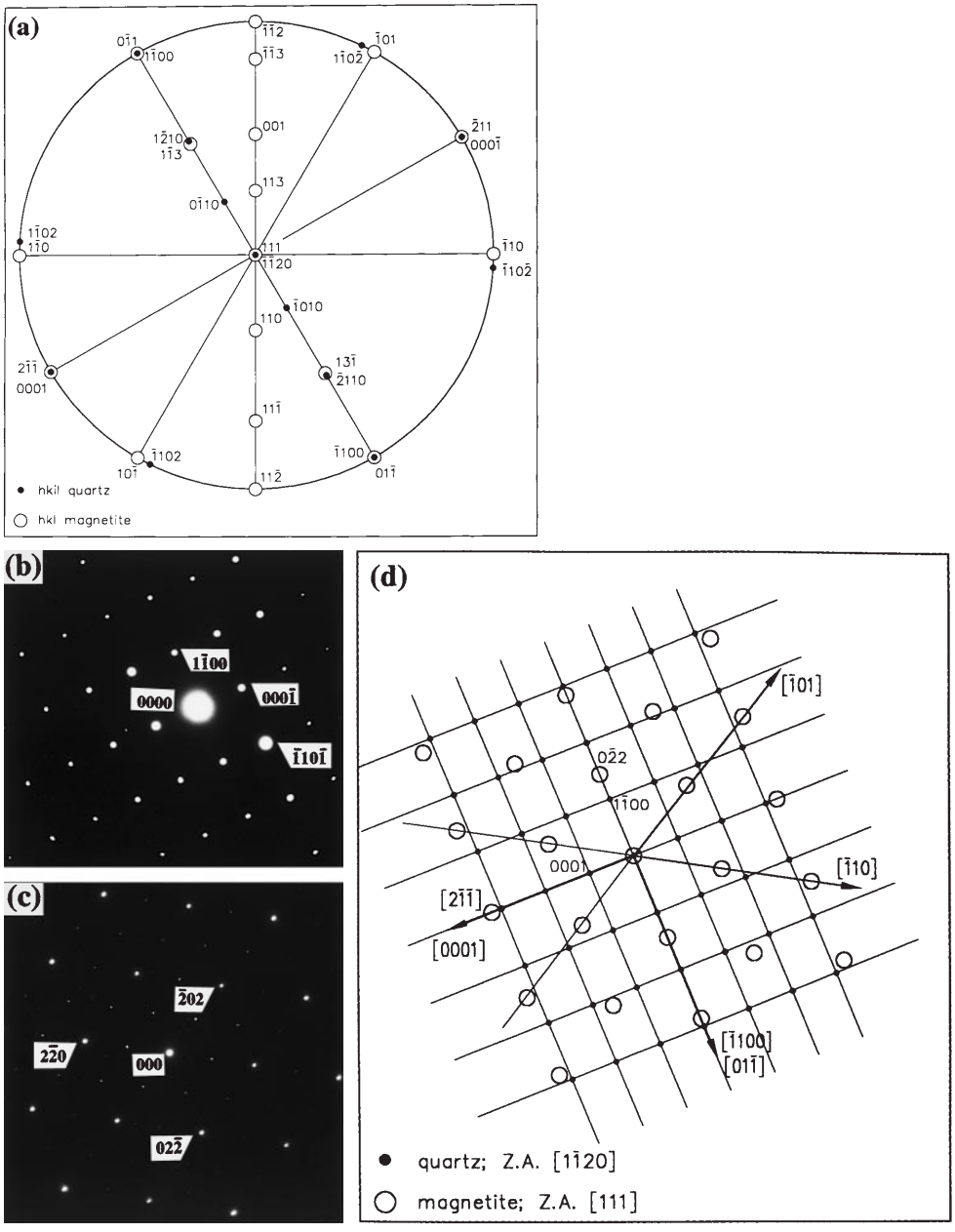


**Fig. 9** **a** Stereographic projection representing orientation relationship II; **b, c** selected area electron diffraction patterns of quartz ZA = [120] and magnetite ZA [111]; **d** schematic diagram of reciprocal lattice coincidences

not to be random, because all three groups share one subparallel ⟨101⟩ direction (Fig. 14b). The particles, therefore, seem to have crystallographic preferred orientation (CPO). Although relatively small, these SEM data are consistent with those of TEM which indicate that the quartz grains of the present study host crystallographically-orientated magnetite particles.

The host quartz grains, however, do not have single orientations but are divided into subgrains, twins and recrystallized grains. In the case of Grain A, two different orientations exist which comprise two twins and two subgrains. The misorientation between the quartz subgrains is 11.5° (Fig. 13c). Quartz grain B comprises 11 subgrains (Fig. 13c), with 4 or 5 different orientations. Thus, although the magnetite crystals across any one of these grains (A or B) have uniform orientation, the orientation relationships between magnetite and quartz from one subgrain to another is variable. It is noteworthy that all the recrystallized quartz have only a limited range of orientations. All the measured subgrains plot into one of 3 broad orientation groups (Fig. 13c).

In addition to magnetite, elemental distribution maps (Fig. 14), identify other phases such as K-feldspar (K + Al + Si + O), biotite (K + Mg + Fe + Al + Si + O), ilmenite (Ti + Fe + O), and REE-bearing minerals along the same planar features. Most of the lamellae shown, however, contain Fe-oxide suggesting a predominance of magnetite. Figure 14c also shows a preponderance of TiFe-oxide occurs in close proximity to the large titanomagnetite grain.

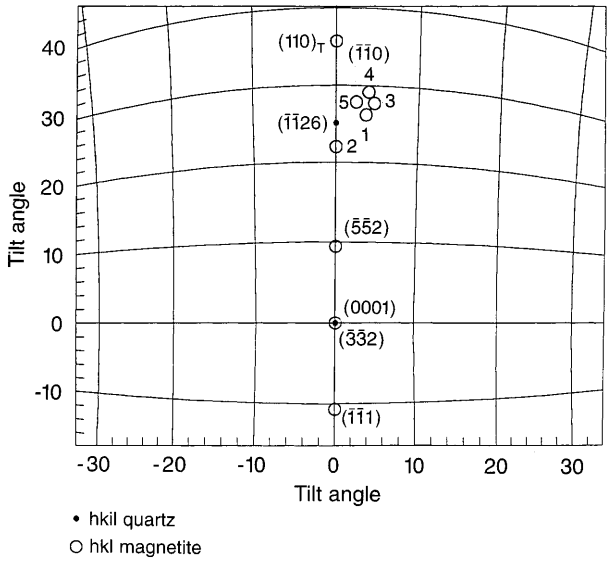


**Fig. 10** Schematic diagram showing relative orientations of *M* (ZA = [110]), with respect with large *Q* (ZA = [0001])

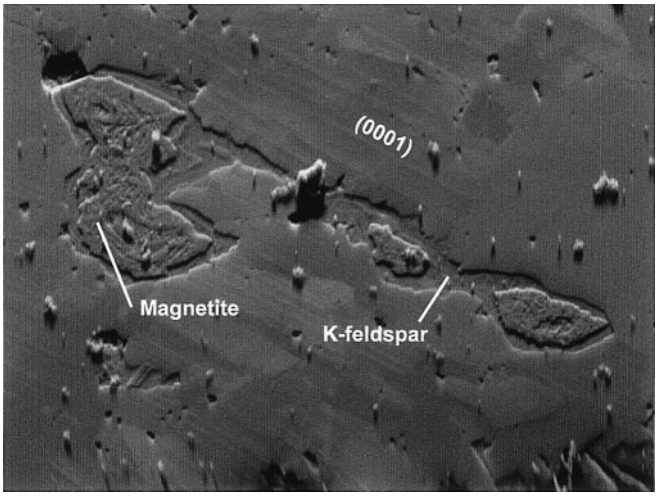


**Fig. 11** Orientation contrast image of magnetite particles aligned parallel to (0001) Brazil twin planar deformation features (*PDF*) in quartz. Note recrystallized quartz replacing quartz containing PDFs. The phase encapsulating magnetite is K-feldspar. The magnetite grains are relatively large, i.e., between 5–10 μm. Width of field of view = 33 μm

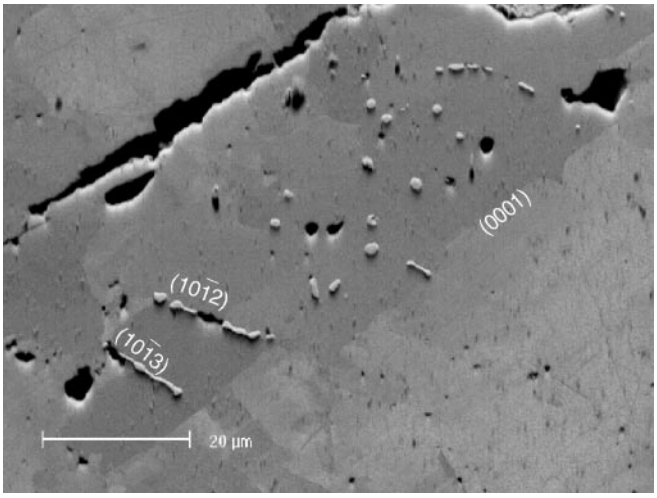


**Fig. 12** Orientation contrast image showing micron-sized equant to elongate *M* in a *Q*. Towards lower left, magnetite particles with high aspect ratios are aligned parallel to the (10$\bar{1}$3) and (10$\bar{1}$2) planes of the host quartz. Sub-perpendicular to this direction (upper left), a partly annealed microfracture parallel to the (0001) plane occurs, also hosting small magnetite particles. Note recrystallized quartz around elongate magnetite no longer exhibits PDFs

Sample VTM1.1

The occurrence of the microcrystalline magnetite in sample VTM1.1 appears to be different from that described for sample KK234. In VTM1.1, the magnetite particles occur either in clusters associated with alteration halos around biotite or in microfractures. Magnetite particles from two quartz grains were found to range between 0.3–7 μm, similar in size to those of KK234. The magnetite particles in quartz grain A ($n$ = 9) generally occur about 5–20 μm from the contact with biotite and are either distributed in small groups or along microfractures. Quartz grain B ($n$ = 3) contains some small (micron-sized) inclusions of biotite and a non-planar healed microfracture partially filled with K-feldspar (Fig. 15). The microfracture is defined by a curvilinear line of inclusions consisting of euhedral K-feldspar, magnetite and hematite, suggesting precipitation from a fluid or melt. The magnetite and hematite particles are grouped together and are surrounded by a rim of K-feldspar (Fig. 15; insert). The crystallographic orientations of the magnetite particles in quartz grains A and B have been determined and show a wide range of orientations (Fig. 16a).

The measurements of 14 magnetite particles inside an albite crystal show 4 to 5 different orientations with high angles of misorientation (Fig. 16b), while the orientations of 4 magnetite particles within chloritic reaction rims around the biotites are all different. Although all the magnetite particles in sample VTM1.1 ($n$ = 30) show a wide range of orientations, they do not have a random distribution. Figure 17 shows the contoured pole plots for the [100], [111] and [101] orientations of all the magnetite measured from VTM1.1. From the contours, it is evident that a preferred orientation exists for the magnetite but without a strong bias.

## MFM results

A quartz grain from sample KK234, containing several magnetite-bearing PDFs (see Figs. 2 and 14a), was investigated by means of MFM. All the lamellae along which the magnetite occur parallel to traces of (0001), (1$\bar{2}$10), (10$\bar{1}$0) and (10$\bar{1}$1) in quartz, determined by electron diffraction analysis, are considered diagnostic of PDF orientations (Grieve et al. 1996). The magnetite

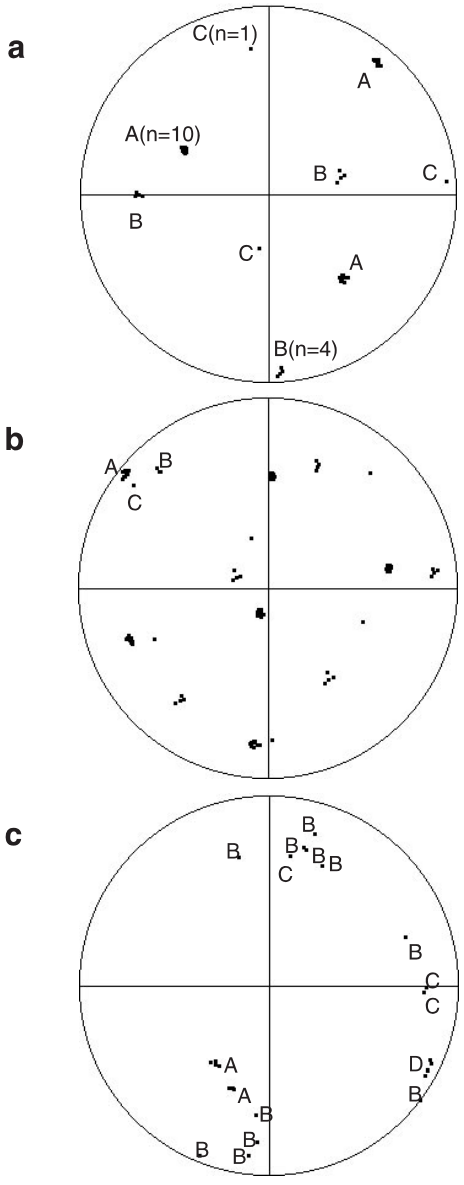


**Fig. 13** **a** Magnetite [100] and **b** [101] pole figures for PDF *M* from three different *Q*: A, B and C. No *M* were measured in *Q* D. Note that in **b** the *M* share one sub-parallel [101] direction. All plots are lower hemisphere equal areas projections and each magnetite crystal appears as three [100] type poles. **c** [0001] pole figure of all quartz grains (A, B, C and D) measured in Sample KK234. Note the limited number of orientations for the quartz grains

particles along (0001) typically have irregular to granular shapes, with low aspect ratio; whereas, those parallel to $(1\bar{2}10)$, $(10\bar{1}0)$ and $(10\bar{1}1)$ have high aspect ratios (Fig. 18a).

The corresponding magnetic force microscopy image shows three types of signals (Fig. 18b). These are:

1. Neutral signals produced by diamagnetic minerals, such as quartz, which consist of even backgrounds with no attractions and repulsion.
2. Multi-domain (MD) signals, produced by the larger ($>0.5$ μm) magnetite grains and those with low aspect ratios. The MD signals are of low intensity (weak) and comprise multiple sets of closely spaced attractive and repulsive zones per individual grain.
3. Single-domain (SD) signals, produced by smaller magnetite particles, with high aspect ratios.
4. A fourth type, a combination of the MD and SD signal types (Pokhil and Moskowitz 1997) is usually referred to as pseudo-single-domain (PSD) magnetite.

The magnetite particles of the centrally situated northeast trending lamellae produces an array of low intensity signals, which reflect the outlines of the magnetite particles shown in the backscatter image (Fig. 18a). The variable and low intensity of the magnetic signals suggest the presence of MD magnetite. In contrast, the magnetite particles from the northwest trending PDF (upper right) produce a conspicuous array of high intensity, alternating attractive and repulsive signals. The high intensity (strong) signals consist of uniformly magnetised grains, which mostly contain only one attraction and repulsion per particle, suggesting presence of SD magnetite particles.

The position, and definition of the attractive signals (e.g., A1 in Fig. 18b) on the MFM image, closely match the outline of the elongate particles (e.g., grain #1) recorded on the backscatter image. This suggests that the particle exposed on the surface of the sample represents one end of a magnetic dipole. The opposite charged end of the dipole (repulsive signal) would then be situated at depth within the sample (e.g., R1, Fig. 18b), consistent with the fact that the repulsive signals are noticeably weaker, broader and more diffuse. This means that the higher amplitude attractive signal's stray field originates at the surface; whereas that of the lower amplitude repulsive signal emanates from depths below the sample surface. The consistent relationships between the origin of the attractive signals at surface and repulsive signals at depth from one grain to another, imply that the dipoles are all magnetized in the same direction. Furthermore, it is observed that the repulsive signals are all noticeably offset to the SSE from that of the attractive signal, implying that the plunge of the magnetic dipoles are subvertical to the surface of the sample. The repulsive and attractive signals are linked by their relative size and shape (e.g., grain #1). However, it is important to note that not all the dipoles in the field of view have uniform plunge. For example, grains #2 and #3 on the backscatter image (Fig. 18a), have their repulsive signals (R2 and R3 respectively) situated in the opposite direction, (i.e., to the NNW).

## Discussion

### Origin of the magnetite along the shock lamellae

Petrographic studies (Hart et al. 1991), from a region of highly shocked granitic samples of the Vredefort structure indicate the presence of microscopic-scale opaque

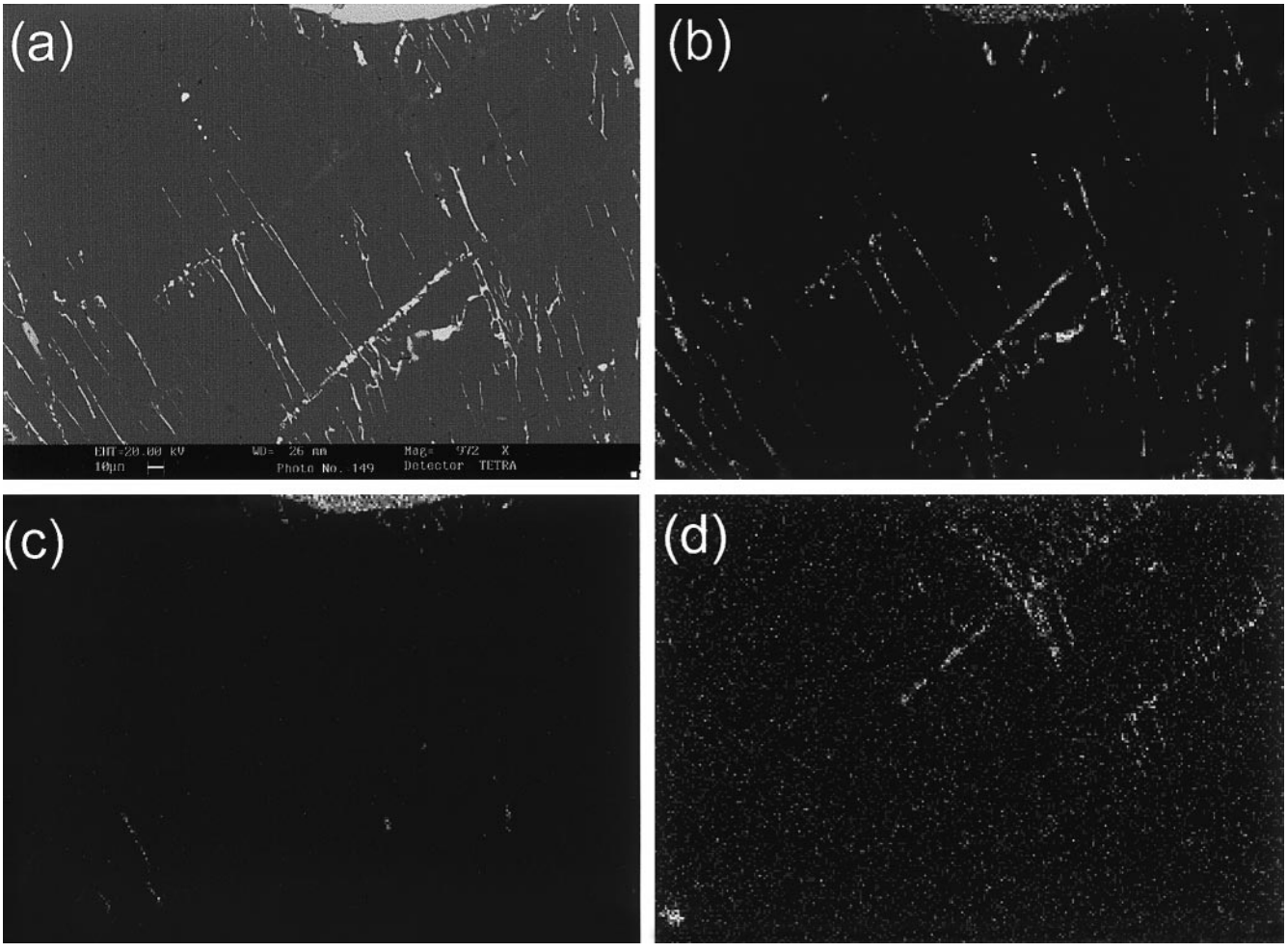


**Fig. 14** **a** Backscatter image of a part of the main area of interest shown in Fig. 2. Element distribution maps **b** Fe, **c** Ti and **d** K show that the PDFs also contain phases other than magnetite. Note the frequency of Ti-rich PDFs close to large TiFe-oxide grain (centre top). Width of field of view = 0.5 mm

phases related to the shock deformation phenomena. The opaque phases occur in several modes but most commonly they are found in planar microfractures within quartz, and as minute grains around flakes of kinked biotite. The application of analytical TEM/STEM and SEM techniques enabled the identification of these microcrystalline opaque phases. Inclusions of various shapes and sizes ranging from approximately 10 nm to micron-size were unambiguously identified as magnetite.

The magnetite in the planar microfractures of quartz occurs along linear arrays parallel to the (0001), $(1\bar{2}10)$, $(10\bar{1}0)$, $(10\bar{1}1)$, $(10\bar{1}2)$ and $(10\bar{1}3)$ planes of quartz. These are considered to be diagnostic of shock orientations, along which *bona fide* PDFs generally develop as a result of impact. However, in the case of Vredefort, most of the PDFs have been eliminated as a result of recovery of silica glass due to the post-shock thermal event (Grieve et al. 1990; Hart et al. 1991; Leroux et al. 1994). Thus, only the magnetite remains as relicts along traces

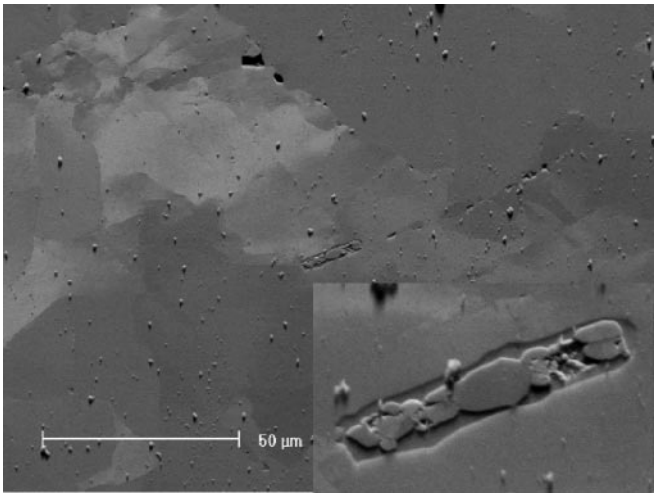


**Fig. 15** An orientation contrast image of typical quartz from Sample VTM1.1 showing a curvilinear healed microfracture. The microfracture is only partly visible because of the non-silica relicts having resisted recrystallization. The largest relict of the microfracture is enlarged in the insert, which shows euhedral magnetite and hematite rimmed by K-feldspar

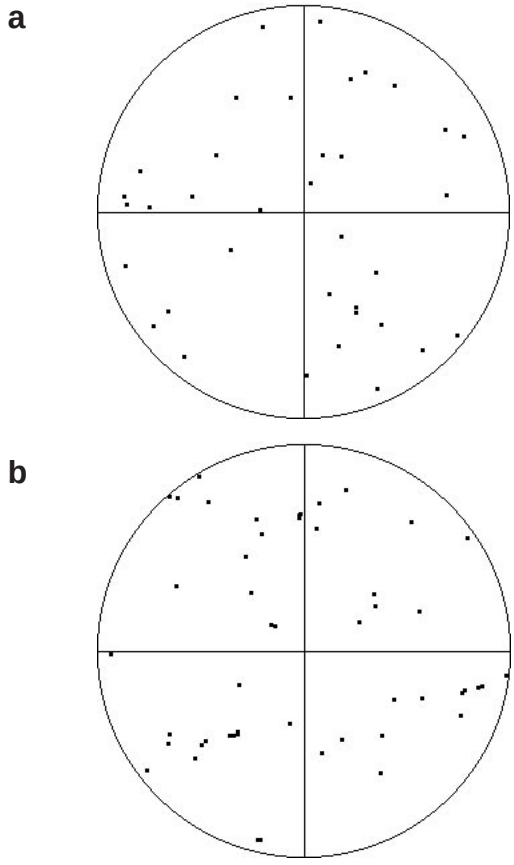


**Fig. 16a, b** Magnetite [100] pole orientations in **a** two *Q* and **b** an albite grain of Sample VTM1.1. Only minor preferred orientation is evident in the albite grain

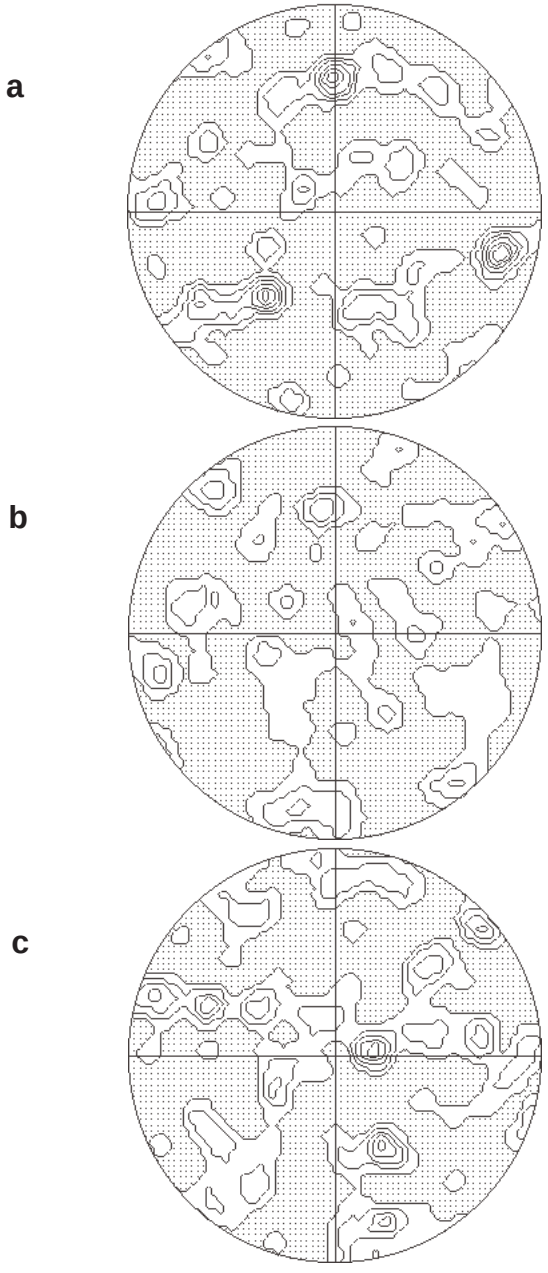


**Fig. 17a–c** Contoured pole figures **a** for [100], **b** for [101] and **c** for [111] of 50 *M* for all submicroscopic *M* inside quartz, albite and biotite for Sample VTM1.1

of the original PDFs. The widths of the relicts (~1 μm) suggests that melting took place along the PDFs, (Langhorst 1994). Provided that the pre-shock temperature of the rocks were around 500 °C (Hart et al. 1991), experimental data suggests that to develop shock lamellae with widths of ~1 μm, shock pressures of about 35 Gpa and temperatures as high as approximately 2400 °C may have been required (Langhorst 1994).

Element distribution maps show other phases, such as K-feldspar, titanite, hematite, ilmenite, biotite, sulphide and REE, are also present with the magnetite, along the PDFs and microfractures (Fig. 15). The distribution of these phases (except magnetite) are notably heterogeneous and patchy and, at most, only one or two are present at any one locality. Silica glass, however, which is not apparent in SEM orientation contrast image (e.g. Fig. 12) because of recovery, is inferred to be ubiquitous along the original Vredefort PDFs. The mineral phases observed along the PDFs are typically those that crystallize from granitic melts, which suggests that the PDFs were intruded by micro-melts derived locally from the surrounding minerals. For example, there is a predominance of TiFe-oxide along the PDFs that occur adjacent to large TiFe-oxide minerals. The micron-sized width of the PDFs is interpreted as indicative of rapid heat dissipation and chilling of intruded micro-melts.

## Crystallographic and magnetic orientations of magnetite

The crystallographic orientations of 36 magnetite particles in five different quartz grains were analysed by electron diffraction using TEM and SEM. In all cases, all the magnetite particles from any one individual quartz grain were found to have identical crystallo-

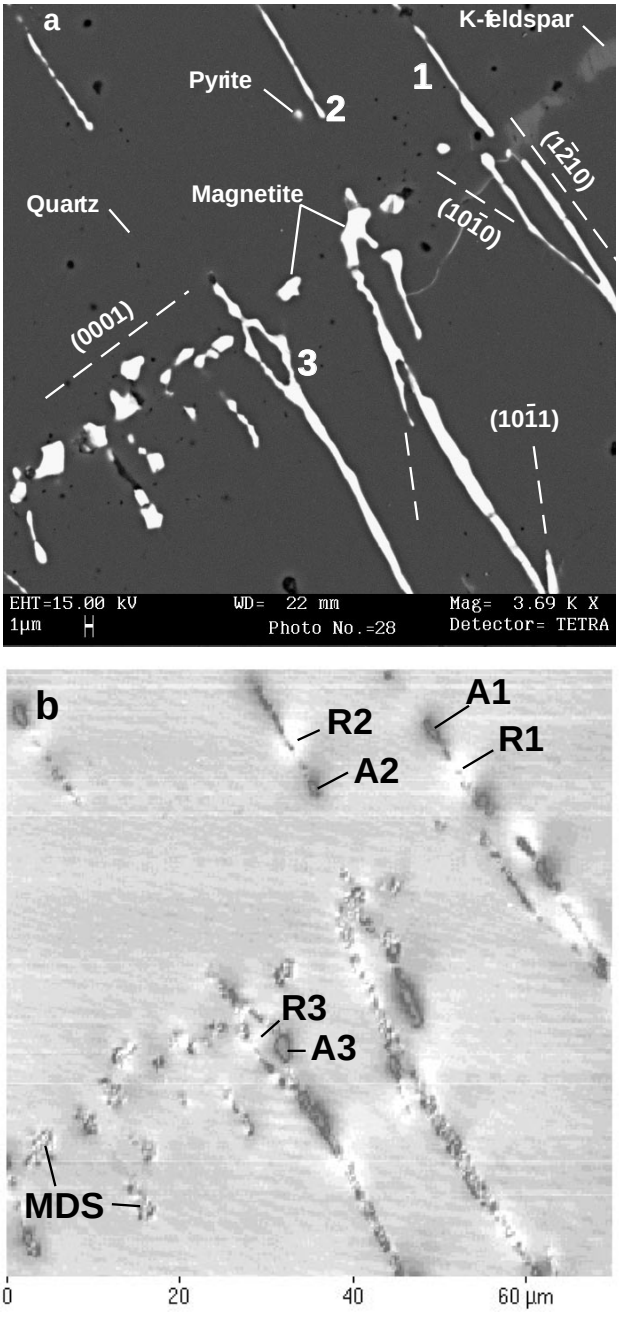


**Fig. 18** **a** Backscatter image of crosscutting sets of magnetite filled relict PDFs set in quartz. The PDF orientations are indicated relative to the quartz host. Note the high aspect ratios of northwest trending magnetite particles, compared to the low aspect ratios of northeast trending particles. **b** magnetic force microscopy (MFM) image of the same area as shown in (**a**). Attractive (*A*) magnetic signals = purple/blue; repulsive (*R*) magnetic signals = orange/yellow; multi-domain signal = *MDS* . Numbers in backscatter image refer to magnetite particles and alpha-numerical labels on the MFM image refer to magnetic signals discussed in text

graphic orientations. Although the orientation of the groups of magnetite varied from one quartz grain to another, the groups seemed systematically misorientated, such that they share a subparallel ⟨101⟩ direction (Fig. 13). This suggests that the magnetite particles have a crystallographic preferred orientations in space, regardless of host quartz orientations. It was also noted that the crystallographic orientation of magnetite in amorphous silica was found to be similar to that observed in one of the nearby quartz crystals. Thus, it would appear that the orientation of magnetite particles had an external control.

In contrast to the magnetite, recrystallized quartz along the PDFs, although not random, exhibit a few (∼3) different orientation groups, which must have developed due to recrystallization during the post-shock thermal event (Fig. 14). Thus, the orientations of the magnetite are unaffected by the growth of new quartz along the PDFs.

It is possible that the magnetite particles could control the orientations of the quartz grains provided crystallization of the magnetite particles preceded the recrystallization of the quartz. Annealing of glass is likely to proceed as a result of the high temperatures achieved during the post-shock thermal event. If the magnetite particle boundaries served as nucleation sites, the crystallographically-orientated magnetite particles could conceivably seed the crystallographic orientations of the newly formed quartz and eventually the orientation of the larger subgrains. Such a mechanism is consistent with the high lattice coincidences, reflected by special orientation relationships I and II, which represent minimum grain boundary energies (cf. Bollman 1970). This would also explain the limited number of orientations of subgrains, twins and recrystallized grains that has been observed (Fig. 13). This interpretation is valid because only a few special orientation relationships would comply with the lowest of minimum energy orientation relationships.

In other instances, the orientations of magnetite particles have been measured in microfractures within quartz, albite and in the alteration halos of biotite grains breaking down to chlorite. In these cases, the micron-sized magnetite particles were found to have a wide range of orientations, with only a minor portion being preferred (Fig. 15). The wide range of orientations and the lack of PDFs in this region (e.g., VTM 1.1) suggests a link between the degree of crystallographic preferred orientations of magnetite and the development of PDFs. Magnetic force imagery of the magnetite particles along the PDFs show well defined arrays of magnetic signals. Intensities of the signals vary with shape and size of the magnetite particles. Magnetite particles larger than about 0.5 μm with low aspect ratios produced weak, complicated, maze-patterned signals, but those <5 μm with high aspect ratios, have high intensity, even-patterned signals comprising single sets of attraction and repulsion. The larger particles are consistent with the description given for MD magnetite; whereas, the <5 μm size particles with high aspect ratios, satisfy the theoretically predicted criteria for single domain magnetite (e.g., Butler 1992).

Offsets of uniform orientations (generally SSE), between the attractive and repulsive signals suggest a

consistent plunge for most of the dipoles (probably less than a third have another direction). The smaller group of particles which have the repulsive signals offset to the NNE (Fig. 18b), as opposed to the SSE of the majority, suggests opposite directions of plunge for the dipoles. The opposite plunge of these dipoles can be explained simply by a switch of magnetization to the diametrically opposing easy axes of the crystallographically oriented magnetite. This is possible because magnetite has four easy directions of magnetization, i.e., the (111) directions, which are at right angles, if viewed along the (001) axis. Despite some of the dipole orientations not being uniform, all SD particles show a uniform vector direction of magnetization, as is suggested by all attractive signals being of higher amplitude than the corresponding repulsive signals. It is evident, therefore, that the systematic alignment of the SD dipoles is controlled by the uniform crystallographic alignment of the magnetite particles. The uniform direction of magnetization seems to suggest an external control.

## Concluding remarks

The results of our study shows that the nature of the PDFs in the Vredefort structure, supposedly diagnostic of impact, are far more complex than previously described. In particular, the occurrence of micro-melts along the approximately 1 μm wide PDFs, which must have intruded during or shortly after the impact event, have not been observed at other impact sites. These observations suggest shock temperatures and pressures far greater than those previously recognised for Vredefort. The magnetite particles associated with the micro-melts appear to have crystallized under special conditions, which enabled them to acquire their preferred crystallographic and magnetic orientations. Their crystallization along the PDFs, has to a large extent controlled their grain size and shape, enabling a large proportion to be SD. Although the cause for the crystallographic and magnetic orientations of the magnetite particles along the PDFs is beyond the scope of this study (see R.J. Hart et al., personal observation), we suggest that the size, shape and orientations of the magnetite particles may have a considerable implication on the magnetic properties of the Vredefort rocks.

**Acknowledgements** We thank Robert Hargraves, Marco Andreoli, Leonie Maré and Deon de Bruin for their continued interest in this work over the years. This investigation was sponsored by the South African Council for Geoscience, and we would like to thank them for allowing us to release the information.

## References

Albat HM (1988) Shatter cone/bedding interrelationship in the Vredefort structure: evidence for meteorite impact? S Afr J Geol 91(1): 106–113

Butler FB (1992) Paleomagnetism. Blackwell Scientific Publications, Boston, pp 319

Carter NL, Officer CB, Drake CL (1990) Dynamic deformation of quartz and feldspar: Clues to causes of some natural crises. Tectonophysics 171: 373–391

Fricke A, Medenbach O, Schreyer W (1990) Fluid inclusions, planar elements and pseudotachylites in the basement of the Vredefort structure, South Africa. Tectonophysics 171: 169–183

Grieve RAF, Coderre JM, Robertson PB, Alexopoulos J (1990) Microscopic planar deformation features in quartz of the Vredefort structure: Anomalous but still suggestive of an impact origin. Tectonophysics 171: 185–200

Grieve RAF, Langenhorst F, Stöffler D (1996) Shock metamorphism of quartz in nature and experiment: II. Significance in geoscience. Meteoritical Soc 31: 6–35

Grütter P, Allenspach R (1994) Can magnetic-force microscopy determine micromagnetic structures? Geophys J Int 116: 502–505

Hargraves RB (1961) Shatter cones in rocks of the Vredefort ring. Geol Soc S Afr Trans 64: 147–153

Hart RJ, Andreoli MAG, Tredoux M, De Wit MJ (1990) Geochemistry across an exposed section of Archaean crust at Vredefort, with implications for mid-crustal discontinuities. Chemical Geology, vol. 82, pp 21–51

Hart RJ, Andreoli MAG, Reimold WU, Tredoux M (1991) Aspects of the dynamic and thermal metamorphic history of the Vredefort structure: implications for its origin. Tectonophysics 192: 313–333

Hart RJ, Hargraves RB, Andreoli MAG, Tredoux M, Doucouré CM (1995) Magnetic anomaly near the centre of the Vredefort structure: implications for impact-related magnetic signatures. Geology 23(3): 277–280

Int. Tables for X-ray Cryst. (1965) Int. Union of Crystallography, Vol. I. Space Group #227, The Kynoch Press, Birmingham

JCPDS, ASTM (1994) PDF-2 file #33–1161, ibid. PDF-2, file #19–629

Langenhorst F (1994) Shock experiments on pre-heated α- and β-quartz: II. X-ray and TEM investigations. Earth Planet Sci Lett 128: 683–698

Leroux H, Reimold WU, Doukhan J-C (1994) A TEM investigation of shock metamorphism in quartz from the Vredefort Dome, South Africa. Tectonophysics 230: 223–239

Martin HJ, Rugar D (1992) Magnetic force microscopy (MFM). In: Wiesendanger R, Güntherodt H-J (eds) Scanning tunneling microscopy II: further applications and related scanning techniques. Springer, Berlin Heidelberg New York, pp 152–207

Martin Y, Wickramasinghe HK (1987) Magnetic imaging by "force microscopy" with 1000 Å resolution. Appl Phys Lett 50: 1455–1457

Martini JEJ (1991) The nature, distribution and genesis of the coesite and stishovite associated with the pseudo-tachylite of the Vredefort Dome, South Africa. Earth Planet Sci Lett 10: 285–300

Nicolaysen LO, Reimold WU (eds) (1990) Proc. Int. Workshop on Crypto Explosions and Catastrophes in the Geological Record, With a Special Focus on the Vredefort structure. Tectonophysics 171 (1–4), p 422

Pokhil TG, Moskowitz BM (1997) Magnetic domains and domain walls in pseudo-single-domain magnetite studied with magnetic force microscopy. J Geophys Res 102B: 22681–22694

Prior DJ, Trimby PW, Weber UD (1996) Orientation contrast imaging of microstructures in rocks using forescatter detectors in the scanning electron microscope. Mineral Mag 60: 859–869

Reimold WU (1990) The controversial microdeformations in quartz from the Vredefort Structure, South Africa- a discussion. S Afr J Geol 93: 645–663

Sutton AP, Balluffi RW (1987) On geometric criteria for low interfacial energy. Acta Metall 35: 2177–2201

Therriault AM, Reid AM, Reimold WU (1993) Original size of the Vredefort structure, South Africa. Lunar Planet Sci 24: 1419–1420